Springer

KSME

Journal of Mechanical Science and Technology 31 (2) (2017) 1003~1013
www.springerlink.com/content/1738-494x(Print)/1976-3824(Online)
DOI 10.1007/s12206-017-0153-x

Numerical simulation of non-Newtonian models effect on hemodynamic factors of pulsatile blood flow in elastic stenosed artery †

Mehdi Jahangiri[1], Mohsen Saghafian[1,*] and Mahmood Reza Sadeghi[2]

[1]*Department of Mechanical Engineering, Isfahan University of Technology, Isfahan, 8415683111, Iran*
[2]*Department of Biomedical Engineering, University of Isfahan, 8174673441, Isfahan, Iran*

(Manuscript Received April 17, 2016; Revised September 7, 2016; Accepted October 1, 2016)

Abstract

Atherosclerosis develops due to different hemodynamic factors, among which time-averaged Wall shear stress (mean WSS) and Oscillatory shear index (OSI) are two of the most important. These two factors not only depend on flow geometry, but are also influenced by rheological characteristics of blood. Since analytical solutions are limited to simple problems and since experimental tests are costly and time consuming, CFD solutions been prominently and effectively used to solve such problems. We conducted a numerical study via ADINA 8.8 software on the non-Newtonian pulsatile flow of blood through an elastic blood artery with single and consecutive stenosis. The studied stenosis cross sectional area was 70 % that of the unstenosed artery. The single stenosis results were compared with the consecutive stenosis results. The five non-Newtonian flow models, the Carreau model, the Carreau-Yasuda model, the modified Casson model, the power-law model, and the generalized power-law model, were used to model the non-Newtonian blood flow. The obtained results showed that increasing the number of stenoses would lead to reduced length of the oscillatory area after the first stenosis, thus forming another oscillatory area with a larger length after the second stenosis. Thus, a consecutive stenosis would develop a larger disease prone area. Upon examining the mean WSS and OSI, we found that, as compared with the other models, the modified Casson model and the power-law model produced predictions for the most extent of damage to endothelial cells and the most disease prone areas, respectively.

Keywords: Adina; Consecutive stenosis; Fluid-solid interaction; Hemodynamic; Reverse flow; Stenosis

1. Introduction

Identifying the areas prone to atherogenesis in the arterial network requires the simultaneous study of mechanical and biomechanical processes. In recent years, certain simplifications have been done for hemodynamic analysis of blood after identifying the areas prone to plaque, and mean certain parameters have been defined for analyzing blood fluids with due consideration of the effect on endothelium of WSS variations. Mean WSS and OSI are two such parameters [1-12]. Van Wyck [13] argued that these parameters can introduce incorrect predictions if the non-Newtonian effects of blood flow are disregarded.

Though the relationship between atherosclerotic and local wall shear stress of blood artery has already been investigated [10-12, 14], and researchers have argued that low shear stress is necessary for plaque formation, shear stress alone cannot correctly predict the location of future plaque formations [15]. Many studies use time-averaged wall shear stress factors as well as the oscillatory shear stress index as indicators for locating the areas prone to atherosclerotic in a blood artery. Some of these articles are discussed below.

Razavi et al. (2006) [16] studied hemodynamic parameters such as mean WSS and OSI in pulsatile blood flow in rigid artery using Quemada and power-law models. Their results of non-Newtonian models compared to Newtonian model revealed that Quemada has a better agreement with experimental results. Also, the power-law and Newtonian models show maximum WSS and maximum OSI, respectively.

Chen and Lu (2006) [17] studied hemodynamic parameters including mean WSS and OSI in pulsatile blood flow in bifurcation, using the non-Newtonian Carreau-Yasuda model. Their results showed that the non-Newtonian characteristics of blood played a significant role in the calculation of the studied parameters.

Rojas (2007) [18] conducted an analytical study on the mean WSS and OSI parameters, using the Thurston model, and obtained a 12 % difference between the OSIs calculated for Newtonian and non-Newtonian blood flows.

Zauskova and Medvidova (2010) [19] used the non-Newtonian Carreau and Yeleswarapu models to study analyti-

*Corresponding author. Tel.: +98 9133101134, Fax.: +98 3133912625
E-mail address: Saghafian@cc.iut.ac.ir
† Recommended by Associate Editor Sung Yang

cally the pulsatile blood flow passing through an elastic blood artery with stenosis. To find the areas prone to atherosclerotic, they examined the mean WSS and OSI parameters. Their results showed that WSS in an elastic blood artery was less than that in a rigid blood artery. They also found that, in a blood artery with stenosis, non-Newtonian models exhibited lower WSS and higher OSI for both elastic and rigid cases.

Sadeghi et al. (2011) [10] studied the effects of stenosis severity on the hemodynamic parameters of blood flow. They used Adina 8.5 software and built a laboratory system. Then the pressure pulses, obtained from the experiments, were used in the simulations. In non-Newtonian and pulsatile blood flow, parameters such as WSS and OSI were obtained and compared for 30 %-80 % symmetrical stenosis. The results showed that until 70 % stenosis, very good agreement was seen between experimental results and numerical data of laminar flow. Also, by change of stenosis severity from 70 % to 80 %, flow became turbulent.

Rikhtegar et al. (2012) [15] studied the OSI parameter in Newtonian blood flow in a rigid blood artery. They used ANSYS CFX for simulation and compared the simulation results with the actual results obtained from 30 patients.

Toloui et al. (2012) [20] used the Carreau-Yasuda model to study the non-Newtonian blood flow through a 3D carotid bifurcation. They also examined the effect of elastic and rigid walls on the WSS to determine if wall elasticity produced a greater effect in this regard than did the blood flow's being non-Newtonian.

Kabinezhadian and Ghista (2012) [21] studied non-Newtonian laminar blood flow during a coronary artery bypass graft. Assuming a linearly elastic blood artery wall, they showed that, as compared to a wall hardened by arteriosclerosis, a flexible wall would produce a maximum 32 % reduction in the mean WSS while somewhat increasing OSI. This reduction of mean WSS in an elastic blood artery was also previously observed in the Refs. [11, 12]. Kabinezhadian and Ghista also argued that wall flexibility and non-Newtonian rheological properties of blood are not independent of each other and, therefore, it is necessary to consider them in quantitative and comparative studies.

Banerjee et al. (2012) [22] studied numerically the effect of different Womersley numbers as well as input waveforms on the mean WSS and OSI in the blood flow through an artery constricted by 50 %. They stated that the existence of stenosis would increase OSI, and that mean WSS and OSI were very much dependent on the input velocity profile. In addition, increasing the Womersley number decreased mean WSS and increased OSI.

Mortazavinia et al. (2012) [23] used the non-Newtonian Carreau model to simulate blood flow in the Aorta by considering the interaction between blood and the blood artery wall. Their results showed that pressure drop in an elastic artery was less than that in a rigid artery, and that a rigid artery would demonstrate a higher WSS than did an elastic artery.

Pereira et al. (2013) [24] simulated three aneurysm models in a rigid carotid artery using ANSYS CFX. They studied the effects of different inlet boundary conditions on the mean WSS and OSI parameters and compared the numerical results with the results obtained from angiography. They predicted the locations with OSI > 0.2 and mean WSS < 1.5 Pa in the blood arteries prone to rupture and fatigue, respectively.

Khader et al. (2014) [25] used ANSYS 13.0 to examine the effect of stenosis severity on WSS in the main branch of an elastic carotid artery. Their simulation results were in good agreement with clinical observations at different percent stenoses.

Van Wyck et al. (2014) [13] studied the WSS and OSI indexes and their effects on predicting the areas prone to developing plaque at a rigid 90-degree arterial-like bifurcations.

Xiang et al. (2014) [26] looked at the effect of input waveform on the computed hemodynamic in four different aneurysm models. Considering the ability of the mean WSS and OSI in extracting biological responses from blood artery wall, they examined the above indexes to predict aneurysm rupture. They subsequently argued that input waveform had little effect on OSI distribution.

Harrison et al. (2014) [27] studied Newtonian blood flow through a rigid carotid bifurcation using Fluent 6.2. Since areas with low WSS are prone to intimal thickening and atherosclerosis, they concluded that areas with WSS < 0.4 Pa and OSI > 0.3 were prone to stenosis growth. Their results showed that a surgeon should avoid excessive dilation of the artery after reconstruction.

Blagojevic et al. (2014) [28] studied blood flow through an elastic coronary bifurcation and examined the roles of OSI and shear stress on the endothelial cells for predicting the occurrence and development of plaque. Their results showed that areas with WSS < 1.5 Pa and very small OSI (zero or near zero) values were prone to genesis of plaque. Also, the lateral walls of the main branch and the lateral walls distal to carina were introduced by them as regions prone to plaque formation.

Gayathri and Shailendhra (2014) [29] examined the WSS and OSI parameters analytically and argued that not only low WSS, but also high OSI played a basic role in locating the areas prone to disease. Their results are in good agreement with those obtained from previous studies.

Meirson et al. (2015) [30] studied the effect of an external stent on the mean WSS and OSI parameters in a saphenous vein graft and its effect on development of intimal hyperplasia. Their results showed that intimal hyperplasia was related to high OSI. Also, in spite of the fact that OSI values in stented patients were considerably lower, their mean WSS indexes were not very different.

Fan et al. (2015) [31] studied the hemodynamic parameters that affected aneurysm rupture in 16 patients using Computational fluid dynamics (CFD). Their results showed that mean WSS was statically significant, whereas OSI did not produce any significant statistical difference.

Since the applications and usefulness of the mean WSS and OSI parameters in non-Newtonian blood flow in consecutive

stenoses of elastic arteries have not yet been studied, and since the abilities of different non-Newtonian models in covering different physical phenomena are different, in the present study were used five non-Newtonian models to study plaque formation as well as to predict the damage incurred on endothelial cells and the extent of the disease-prone areas. In addition, to study the effect of the non-Newtonian nature of the blood on the examined parameters, the Newtonian model also was used.

2. Governing equations

In ADINA 8.8 software, momentum and continuity equations are as follows [32]:

$$\frac{\partial(\rho V)}{\partial t}+\nabla.(\rho VV-\tau)=f_B \tag{1}$$

$$\frac{\partial \rho}{\partial t}+\nabla.(\rho V)=0 \tag{2}$$

where t is time, ρ is density, V is the velocity vector, f_B is the volume force vector acting on the fluid, and τ is the stress tensor calculated as follows:

$$\tau=-pI+2\mu e \tag{3}$$

$$e=\frac{1}{2}(\nabla V+\nabla V^T) \tag{4}$$

where p is pressure, I is the unit matrix, and μ is the fluid viscosity.

3. Non-Newtonian models

Five non-Newtonian and one Newtonian model were used to model the fluid behavior. The formulas and their constants are presented in Table 1 in detail. The constants were obtained by various researchers through fitting the experimental data of blood [33]. The relationship between viscosity and shear rate for the Newtonian model and the five non-Newtonian models is shown in Fig. 1. As shown, the power-law model tends to zero at high shear rates. Although it is generally accepted that at shear rates greater than 100/s blood acts as a Newtonian fluid [34, 35], the advantage of the power-law model lies in the simplicity of its formula. At high shear rates (sufficiently greater than 100/s), the Carreau viscosity model is similar to the Newtonian viscosity model. Cho and Kensey [36] stated that this model showed a good agreement with experimental data. The Carreau-Yasuda model is similar to the Carreau model, but tends to Newtonian viscosity at lower shear rates than does the Careau model. However, even this lower shear rate is large to be acceptable for Newtonian behavior [33]. The advantage of the Casson model is that it takes into account blood yield stress [37]. Since the Casson model becomes divergent as shear rate tends to zero, therefore modified Casson model is proposed. The modified Casson model proposes higher values for viscosities at conditions close to Newtonian conditions and lower values for low shear rates [38]. The generalized power-law model is an extension of the power-law model. At low shear rates, this model behaves like the power-law model, and at medium and high shear rates (greater than 200/s), it acts as a Newtonian model. In addition, in a wide range of low shear rates (0.5/s-50/s), this model exhibits a similar behavior to the Carreau model [33].

Table 1. Non-Newtonian models for viscosity of blood.

$\mu=0.0033$	Newtonian [10]
$\mu=k\lvert\dot{\gamma}\rvert^{n-1}\quad k=0.035,\ n=0.6$	Power-law [36]
$\mu=\mu_\infty+(\mu_0-\mu_\infty)\left(1+A\lvert\dot{\gamma}\rvert^2\right)^n$ $A=10.976,\ n=-0.3216,\ \mu_\infty=0.0033,\ \mu_0=0.056$	Carreau [36]
$\mu=\mu_i+\frac{\mu_0-\mu_i}{\left[1+(\lambda\lvert\dot{\gamma}\rvert^b)\right]^a}$ $\mu_0=0.016,\ \mu_i=0.0033,\ \lambda=8.2,$ $b=1.23,\ a=0.64$	Carreau-Yasuda [39]
$\mu=\left[\sqrt{\tau_y\left(\frac{1-e^{-m\lvert\dot{\gamma}\rvert}}{\lvert\dot{\gamma}\rvert}\right)}+\sqrt{\mu_c}\right]^2$ $\mu_c=0.0033,\ m=100$	Modified-Casson [40]
$\mu=k(\dot{\gamma})\lvert\dot{\gamma}\rvert^{n(\dot{\gamma})-1}$ $k(\dot{\gamma})=\mu_\infty+\Delta\mu\ \exp\left[-(1+\frac{\lvert\dot{\gamma}\rvert}{a})\exp(\frac{-b}{\dot{\gamma}})\right]$ $n(\dot{\gamma})=n_\infty-\Delta n\ \exp\left[-(1+\frac{\lvert\dot{\gamma}\rvert}{c})\exp(\frac{-d}{\dot{\gamma}})\right]$ $\mu_\infty=0.0033,\ \Delta\mu=0.25,\ n_\infty=1,\ \Delta n=0.45$ $a=50,\ b=3,\ c=50,\ d=4$	Generalized power-law [41]

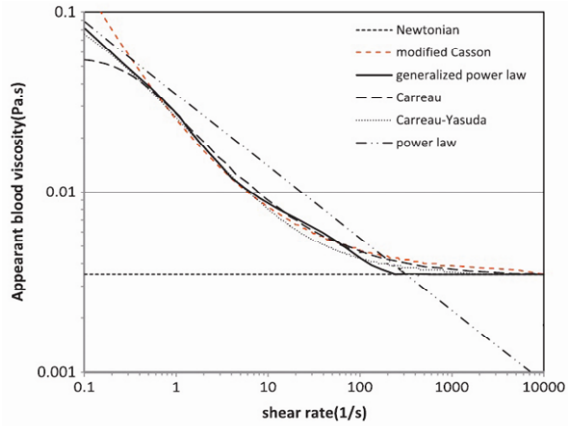

Fig. 1. Viscosities versus shear rate for non-Newtonian models.

4. Present work and numerical methods

An elastic artery with a 70 % symmetrical single and consecutive stenosis was studied here. Dimensions are shown in

Table 2. Characteristics blood and artery wall.

Blood	Artery wall			
Density (kg/m^3)	Poisson ratio	Density (kg/m^3)	Elasticity modulus (kPa)	Thickness (m)
1050	0.49	1300	910	0.0005

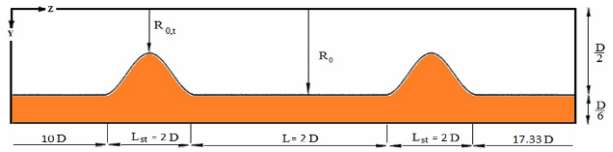

Fig. 2. Computational domain for an artery with consecutive stenosis.

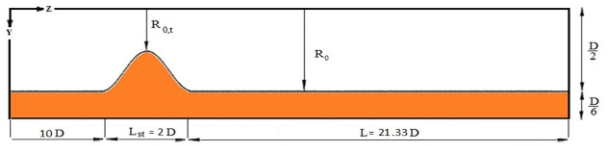

Fig. 3. Computational domain for an artery with single stenosis.

Figs. 2 and 3.

The equation of the stenosed region of the artery is [10-12]:

$$\frac{R(z)}{R_0} = 1 - \left(\frac{R_0 - R_{0,t}}{2R_0}\right)\left(1 + \cos\frac{2\pi(z - z_m)}{L_{st}}\right) \quad (5)$$

where R_0 is the healthy artery radius, R(z) is the artery radius in the stenosed region, $R_{0,t}$ is the artery radius at the stenosis throat, z_m is the axial coordinates of the stenosis throat with respect to the origin, and L_{st} is the length of the stenosed region. Fluid and artery wall properties are listed in Table 2 [10-12].

Artery wall displacement and strain was considered large in the kinematic formulation. At the two ends of the fluid and solid models, axial and radial displacements were constrained. Boundary condition of zero normal stress was imposed on the outer wall of the artery, assuming that the surrounding tissues do not exert any external or pressure forces on the artery wall [42].

Fig. 4 shows the average velocity profiles applied on the inlet boundary condition [43]. Time, in Fig. 4, has become dimensionless with heart fluctuation period which is 0.8 s.

FSI boundary condition was used in the fluid-solid interface. The governing equations for the solid-fluid coupling are [10-12]:

$$d_f = d_s \text{ : Displacement} \quad (6)$$

$$n.\sigma_f = n.\sigma_s \text{ : Traction} \quad (7)$$

$$\dot{d}_f = \dot{d}_s \text{ : No slip} \quad (8)$$

where d, σ and n are displacement vector, stress tensor, and the normal vector, respectively. The governing equation of the

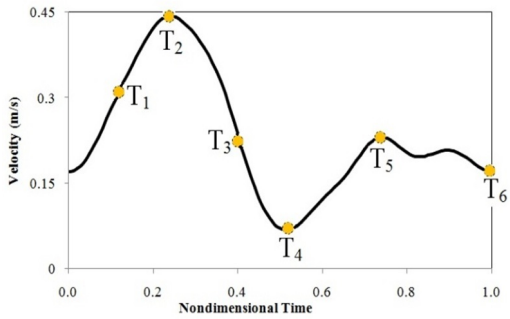

Fig. 4. Inlet velocity pulse.

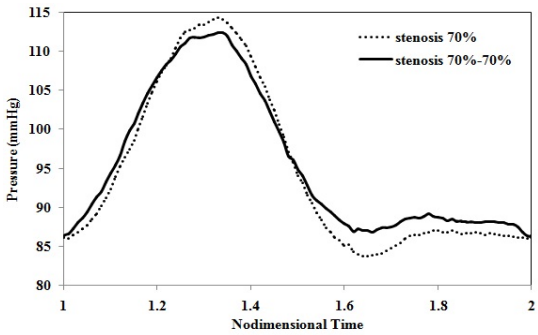

Fig. 5. Blood pressure pulses that used as the output condition.

solid domain is [10-12]:

$$\rho_s \ddot{d}_s = \nabla_\circ.\sigma_s + \rho_s f_s \quad (9)$$

where ρ_s is the wall density, σ_s is the Cauchy stress tensor, f_s is the volume force vector, and d_s is the wall displacement vector.

As shown in Fig. 5, when a solid-fluid coupling problem is investigated, the blood pressure pulses that are obtained in vitro [10] must be applied as the output condition.

Grid independency of results was examined to obtain grid-independent results to determine the best results and to minimize computer running-time. Three inlet velocity pulses were considered to achieve stable and convergent solutions [14]. The simulations were performed on a computer equipped with a 2.93 GHz processor and 8 G of RAM.

5. Results

Mean inlet pressure for different stenosis percentages in two cases of single and consecutive stenosis is shown in Figs. 6 and 7. For stenosis with a severity of up to 70 %, a very good agreement was observed between the experimental results [10] and the laminar flow assumption, suggesting a laminar flow in the stenosis less that 70 %. The results of Figs. 6 and 7 show that the laminar flow assumption is reasonable for stenosis with severities of less that 70 %.

The OSI is determined as the transient characteristic of the flow as [11, 12]:

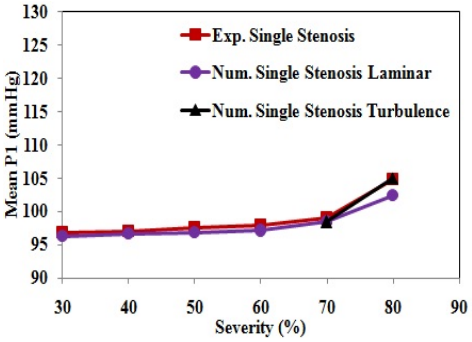

Fig. 6. Mean input pressure for different % of single stenosis.

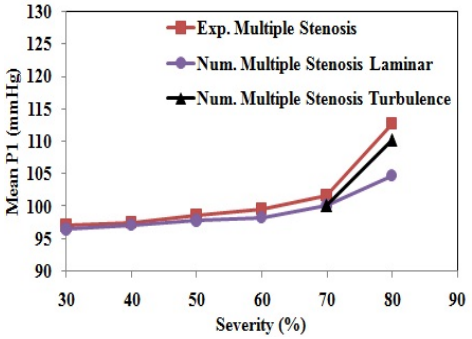

Fig. 7. Mean input pressure for different % of consecutive stenosis.

$$OSI = \frac{1}{2} \times \left(1 - \frac{\left| \int_0^T \tau_w \, dt \right|}{\int_0^T \left| \tau_w \right| dt}\right). \quad (10)$$

OSI values vary between 0 and 0.5, and are affected by separation and reattachment points. Figs. 8 and 9 show the OSI for 70 % and 70 %-70 %, as well as the different rheological models used for blood. As can be seen in Fig. 8, there are two maxima, one coinciding with the time-averaged separation point and the other coinciding with the time-averaged flow reattachment point. As shown in Fig. 9, there are four maxima: the first coinciding with the first time-averaged separation point, the second coinciding with the time-averaged reattachment flow behind the first stenosis, the third coinciding with the second time-averaged separation point, and the fourth coinciding with the time-averaged flow reattachment point behind the second stenosis.

Time-averaged shear stress is defined as:

$$Mean WSS = \frac{1}{T} \int_0^T \tau_w \, dt \quad (11)$$

where T is the cardiac cycle period and τ_w is the shear stress vector.

Figs. 10 and 11 show the mean WSS at 70 % and 70 %-70 % stenosis cases obtained from five different non-Newtonian models and compare them with that obtained from

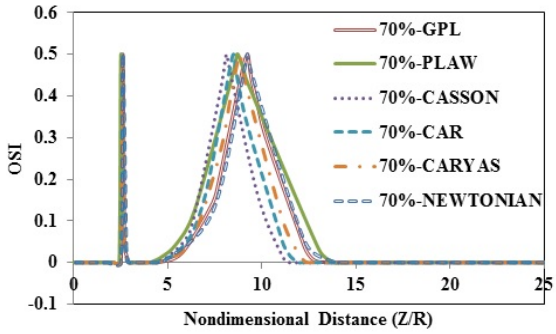

Fig. 8. OSI, 70 % stenosis.

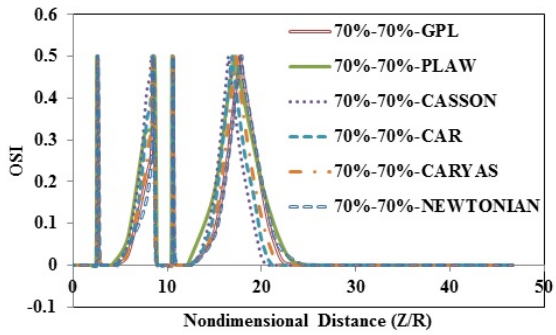

Fig. 9. OSI, 70 %-70 % stenosis.

the Newtonian model. As can be observed, in the area before the stenosis, the mean WSS is not as sensitive as the non-Newtonian model. In all the models, mean WSS increased in the proximal stenosis area. Such increase can lead to increased production of nitric oxide by endothelial cells [44]. Nitric oxide protects these cells from cellular death, leading to their proliferation for covering the plaque surface during the development of the plaque. In addition, the mean WSS diagrams showed that mean WSS also decreased in the area after the stenosis, while a reverse flow was formed and developed in the area after the stenosis.

In Figs. 10 and 11, the Carreau, Carreau-Yasuda, and modified Casson models show somewhat greater shear stresses than does the Newtonian model in the areas before and after the stenosis. At the throat of stenosis where shear rate increases dramatically, however, the non-Newtonian models show shear stresses close to that of the Newtonian model, and exhibit good sensitivity as compared with the non-Newtonian properties of blood. The generalized power-law model also shows shear stress values close to the Newtonian model, but the shear rate of power-law model before and after the stenosis is - as opposed to the other models - lower than that obtained from the Newtonian model. In addition, the shear stress at the stenosis throat is less than that of the Newtonian model, which cannot be a correct result.

Based on Figs. 8-11, the results show that the modified Casson non-Newtonian model - due to its highest mean WSS - would predict more severe damage to endothelial cells. In addition; the non-Newtonian power-law model - due to its

Table 3. Comparison of Mean WSS as well as oscillatory and reverse flow area lengths obtained from different non-Newtonian models.

Model	Max. Mean WSS		Min. Mean WSS		Reverse flow area lengths (Z/R)			Oscillatory flow area lengths		
	Second	First	Second	First	Total	Second	First	Total	Second	First
Newtonian, 70 %	-	34.375	-	-1.804	6.583	-	6.583	10.418	-	10.418
Newtonian, 70 %-70 %	31.838	34.346	-1.695	-1.805	13.148	7.145	6.003	17.443	12.901	4.542
Carreau, 70 %	-	34.899	-	-1.834	5.742	-	5.742	8.165	-	8.165
Carreau, 70 %-70 %	32.478	34.872	-1.68	-1.805	11.892	6.142	5.75	15.458	10.434	5.024
Carreau-Yasuda, 70 %	-	34.564	-	-1.82	6.113	-	6.113	8.390	-	8.39
Carreau-Yasuda, 70 %-70 %	32.09	34.541	-1.712	-1.82	12.446	6.542	5.904	15.527	10.693	4.834
Power-law, 70 %	-	14.07	-	-1.665	6.211	-	6.211	11.069	-	11.069
Power-law, 70 %-70 %	13.23	14.08	-1.526	-1.623	12.792	6.642	6.15	21.327	15.720	5.607
Gen. power-law, 70 %	-	34.528	-	-1.816	6.485	-	6.485	9.928	-	9.928
Gen. power-law, 70 %-70 %	31.98	34.49	-1.704	-1.816	13.140	7.145	5.995	17.215	12.372	4.843
Modified Casson, 70 %	-	35.479	-	-1.847	5.558	-	5.558	7.719	-	7.719
Modified Casson, 70 %-70 %	33.096	35.432	-1.76	-1.846	11.692	5.942	5.75	14.050	8.945	5.105

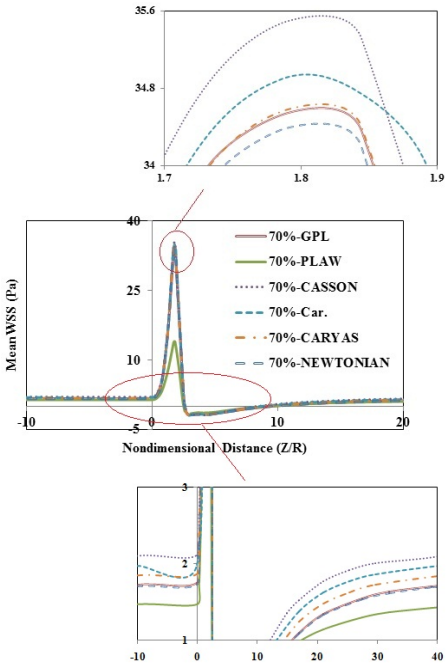

Fig. 10. Mean WSS, 70 % stenosis.

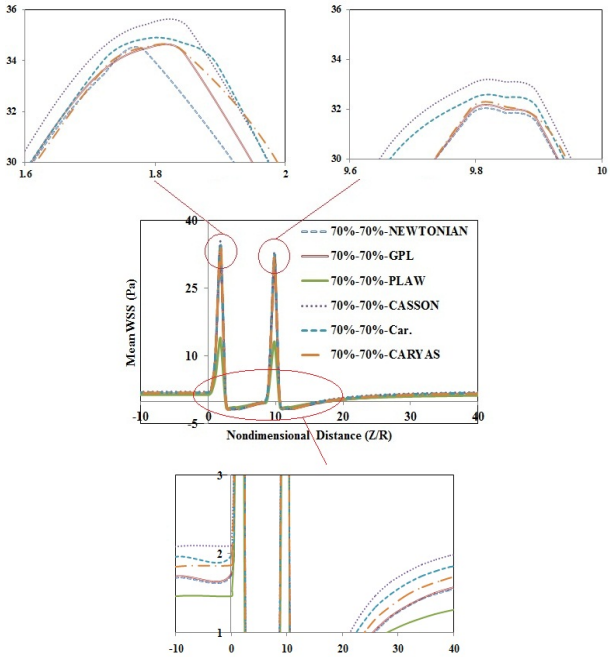

Fig. 11. Mean WSS, 70 %-70 % stenosis.

maximum length of oscillatory area - would predict a greater disease prone area than do other models.

Table 3 shows the minimum and maximum mean WSS, oscillatory area length, and reverse flow area lengths obtained from different non-Newtonian models at 70 % and 70 %-70 % stenoses.

From Figs. 10 and 11 and Table 3, the results show that, at consecutive stenosis, shear stress on the second stenosis is less than that on the first. The reason is that blood flow, upon passing the first stenosis, is diverted towards the blood artery central axis, thus increasing the speed along this axis at the site of the second stenosis, leading to reduced velocity gradient at the wall which in turn reduces shear stress. In addition, since, at consecutive stenosis, the dilation of the artery wall is greater than that in single stenosis, the maximum shear stress for single stenosis is slightly greater than that in consecutive stenosis. Another observation was that the power-law model produced the least maximum mean WSS. This can be explained from the viscosity - shear rate diagram where the power-law model exhibits lower viscosity at higher shear rates.

The greatest length of reverse flow area (Table 3) was obtained from the Newtonian model and the least from the modified Casson model. Since low mean WSS increases LDL particle diffusivity into the wall by affecting cellular secretions [45], non-Newtonian blood flow would reduce the probability of formation of a new stenosis after the second stenosis.

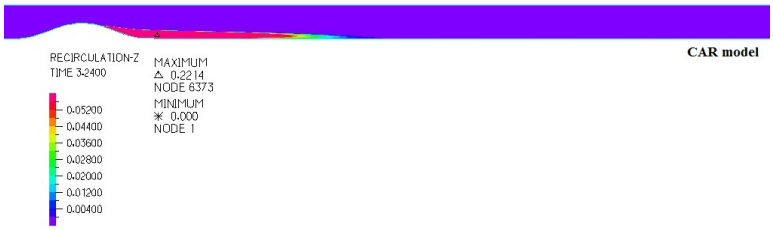

Fig. 12. Reverse flow region, 70 % stenosis, Carreau model.

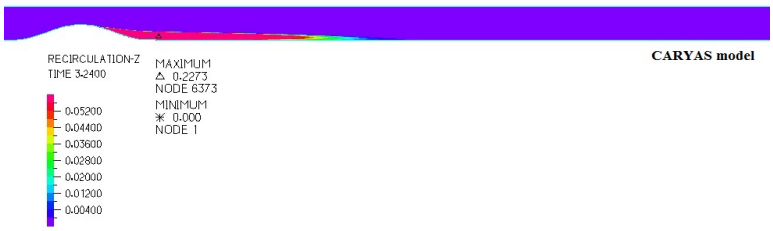

Fig. 13. Reverse flow region, 70 % stenosis, Carreau-Yasuda model.

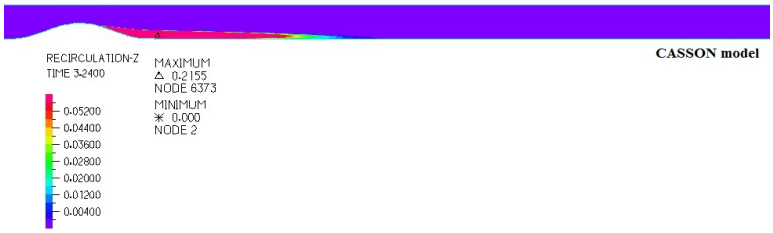

Fig. 14. Reverse flow region, 70 % stenosis, modified Casson model.

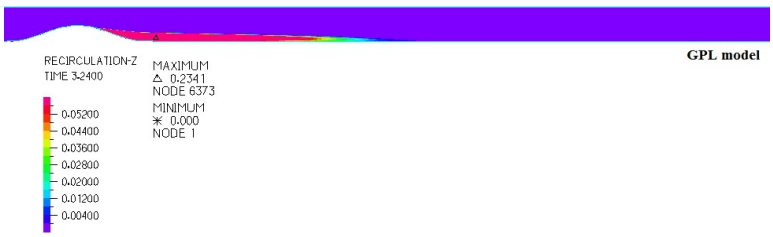

Fig. 15. Reverse flow region, 70 % stenosis, generalized power-law model.

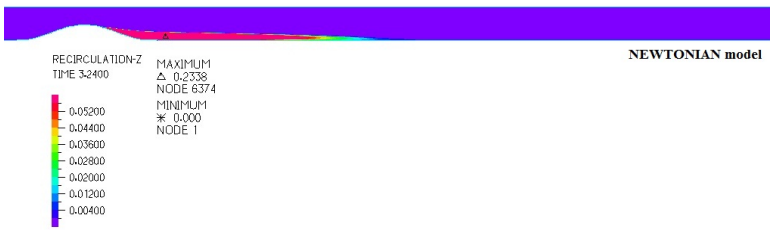

Fig. 16. Reverse flow region, 70 % stenosis, Newtonian model.

As shown in Table 3, conversion of a single stenosis into a consecutive stenosis would lead to reduced length of the oscillatory area after the first stenosis, thus forming another oscillatory area with a larger length after the second stenosis. Thus, a consecutive stenosis would develop a larger disease prone area. In addition, considering the length of the reverse flow area, conversion of a single stenosis into a consecutive stenosis using the Newtonian, Carreau-Yasuda, power-law, and generalized power-law models, would increase the growth rate of the first stenosis. In the modified Casson and Carreau models, however, the growth rate of the first stenosis is reduced. In addition, with due consideration of the increased length of the reverse flow area after the second stenosis in all the models, the results showed that the probability of a new stenosis form-

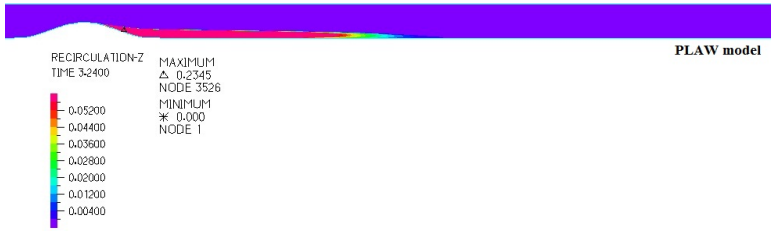

Fig. 17. Reverse flow region, 70 % stenosis, power-law model.

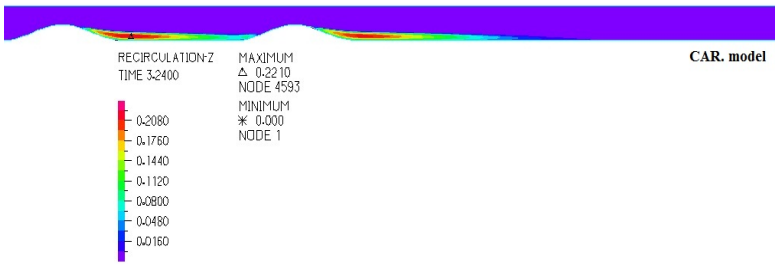

Fig. 18. Reverse flow region, 70 %-70 % stenosis, Carreau model.

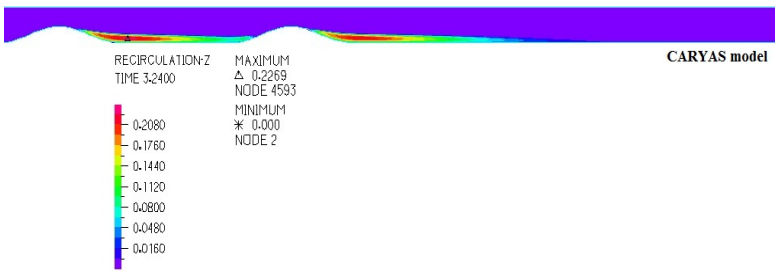

Fig. 19. Reverse flow region, 70 %-70 % stenosis, Carreau-Yasuda model.

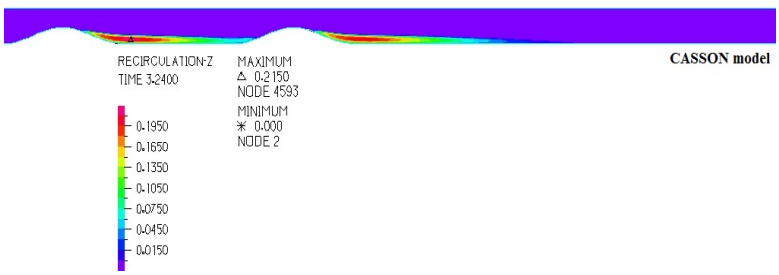

Fig. 20. Reverse flow region, 70 %-70 % stenosis, modified Casson model.

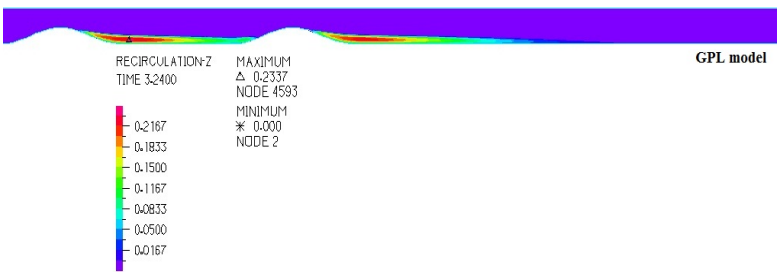

Fig. 21. Reverse flow region, 70 %-70 % stenosis, generalized power-law model.

ing after the second would increase in all the models.

Figs. 12-17 show the reverse flow contours obtained at maximum flow rate (T_2) for 70 % stenosis from different non-Newtonian models as well as the Newtonian model. As can be observed, the power-law model produces the greatest and the modified Casson model produces the least length for the re-

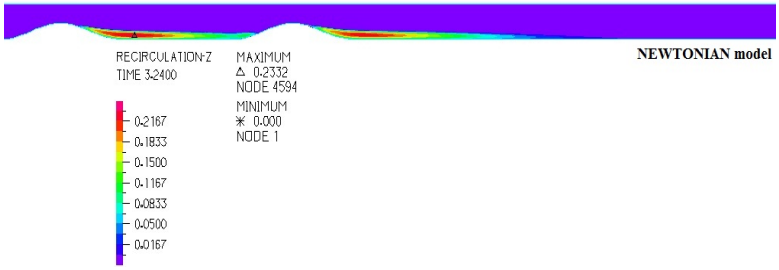

Fig. 22. Reverse flow region, 70 %-70 % stenosis, Newtonian model.

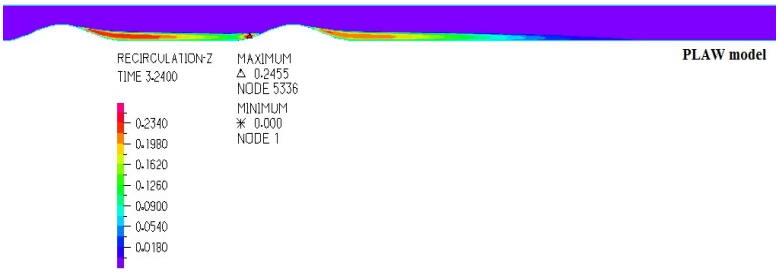

Fig. 23. Reverse flow region, 70 %-70 % stenosis, power-law model.

verse flow area behind the stenosis. In all the models except the power-law, maximum reverse flow occurs at behind of stenosis. However, in the power-law model, the maximum reverse flow rate occurs at the distal of the stenosis.

Figs. 18-23 show the reverse flow area contours at maximum flow rate for 70 %-70 % stenosis, obtained from the non-Newtonian as well as the Newtonian models. As can be seen, the greatest and least lengths of the reverse flow area are obtained from the power-law and modified Casson models, respectively. This result is in good agreement with the results obtained in our previous studies [14]. At a 70 %-70 % stenosis, as can be observed in the figures, the reverse flow area after the first stenosis continues until as far as the throat of the second stenosis. In all the models except the power-law model, the maximum flow rate occurs after the first stenosis, whereas in the power-law model, this maximum occurs immediately before the second stenosis.

6. Conclusion

It is believed that hemodynamics plays a great role in locating vascular disease formation in such areas as carotid artery, coronary artery, and bifurcations. For this reason, researchers have endeavored to find the areas prone to developing arthrosclerosis by studying such hemodynamic parameters as mean WSS and OSI, arguing that, for locating disease prone areas, these two parameters must be examined simultaneously. For this reason, in this paper numerical simulation was done for study of the mean WSS and OSI parameters in an elastic blood artery subjected to pulsatile blood flow. ADINA 8.8 software and five non-Newtonian models were used for simulating at 70 % and 70 %-70 % stenosis condition. The obtained results for single and consecutive stenosis cases were compared. Considering the length of the time-averaged reverse flow area, the results showed that the non-Newtonian properties of the blood would reduce the probability of a new stenosis being formed beyond the second stenosis.

References

[1] C. Zarins, D. Giddens, B. Bharadvaj, V. Sottiurai, R. Mabon and S. Glagov, Carotid bifurcation atherosclerosis. Quantitative correlation of plaque localization with flow velocity profiles and wall shear stress, *Circ. Res.*, 53 (4) (1983) 502.

[2] D. Ku, D. Giddens, C. Zarins and S. Glagov, Pulsatile flow and atherosclerosis in the human carotid bifurcation. Positive correlation between plaque location and low oscillating shear stress, *Arterioscler. Thromb. Vasc. Biol.*, 5 (3) (1985) 293-302.

[3] E. Pedersen, S. Oyre, M. Agerbaek, I. Kristensen, S. Ringgaard, P. Boesiger and W. Paaske, Distribution of early atherosclerotic lesions in the human abdominal aorta correlates with wall shear stresses measured in vivo, *Eur. J. Vasc. Endovasc. Surg.*, 18 (4) (1999) 328-333.

[4] M. Lei, D. Giddens, S. Jones, F. Loth and H. Bassiouny, Pulsatile flow in an end-to-side vascular graf tmodel: comparison of computations with experimental data, *J. Biomech. Eng.*, 123 (2001) 80.

[5] J. Soulis, G. Giannoglou, G. Parcharidis and G. Louridas, Flow parameters in normal left coronary artery tree. Implication to atherogenesis, *Comput. Biol. Med.*, 37 (5) (2007) 628-636.

[6] J. Soulis, G. Giannoglou, Y. Chatzizisis, K. Seralidou, G. Parcharidis and G. Louridas, Non-newtonian models for molecular viscosity and wall shear stress in a 3d reconstructed human left coronary artery, *Med. Eng. Phys.*, 30 (1) (2008)

9-19.

[7] J. R. Cebral, F. Mut, J. Weir and C. M. Putman, Association of hemodynamic characteristics and cerebral aneurysm rupture, *Am. J. Neuroradiol.*, 32 (2011) 264-270.

[8] G. Lu, L. Huang, X. L. Zhang, S. Z. Wang, Y. Hong, Z. Hu and D. Y. Geng, Influence of hemodynamic factors 356 on rupture of intracranial aneurysms: patient-specific 3D mirror aneurysms model 357 computational fluid dynamics simulation, *Am. J. Neuroradiol.*, 32 (2011) 1255-1261.

[9] J. Xiang, S. K. Natarajan, M. Tremmel, D. Ma, J. Mocco, L. N. Hopkins, A. H. Siddiqui, E. I. Levy and H. Meng, Hemodynamic-morphologic discriminants for intracranial aneurysm rupture, *Stroke*, 42 (2011) 144-152.

[10] M. R. Sadeghi, E. Shirani, M. Tafazzoli-Shadpour and M. Samaee, The effects of stenosis severity on the hemodynamic parameters-assessment of the correlation between stress phase angle and wall shear stress, *J. Biomech.*, 44 (15) (2011) 2614-2626.

[11] M. Jahangiri, M. Saghafian and M. R. Sadeghi, Numerical study of turbulent pulsatile blood flow through stenosed artery using fluid-solid interaction, *Comput. Math. Methods Med.* (2015) Article ID 515613.

[12] M. Jahangiri, M. Saghafian and M. R. Sadeghi, Numerical simulation of hemodynamic parameters of turbulent and pulsatile blood flow in flexible artery with single and double stenoses, *J. Mech. Sci. Technol.*, 29 (8) (2015) 3549-3560.

[13] S. Van Wyk, L. P. Wittberg and L. Fuchs, Atherosclerotic indicators for blood-like fluids in 90-degree arterial-like bifurcations, *Comput. Biol. Med.*, 50 (2014) 56-69.

[14] M. Jahangiri, M. Saghafian and M. R. Sadeghi, Effects of non-Newtonian behavior of blood on wall shear stress in an elastic vessel with simple and consecutive stenosis, *Biomed. Pharmacol. J.*, 8 (1) (2015) 123-131.

[15] F. Rikhtegar, J. A. Knight, U. Olgac, S. C. Saur, D. Poulikakos, W. Marshall, P. C. Cattin, H. Alkadhi and V. Kurtcuoglu, Choosing the optimal wall shear parameter for the prediction of plaque location-A patient-specific computational study in human left coronary arteries, *Atherosclerosis*, 221 (2) (2012) 432-437.

[16] M. R. M. Razavi, S. H. Seyedein and P. B. Shahabi, Numerical study of hemodynamic wall parameters on pulsatile flow through arterial stenosis, *IUST International Journal of Engineering Science*, 17 (3-4) (2006) 37-46.

[17] J. Chen and X. Y. Lu, Numerical investigation of the non-Newtonian pulsatile blood flow in a bifurcation model with a non-planar branch, *J. Biomech.*, 39 (2006) 818-832.

[18] H. A. G. Rojas, Numerical implementation of viscoelastic blood flow in a simplified arterial geometry, *Med. Eng. Phys.*, 29 (4) (2007) 491-496.

[19] A. Hundertmark-Zauskova and M. Lukacova-Medvidova, Numerical study of shear-dependent non-Newtonian fluids in compliant vessels, *Comput. Math. with Appl.*, 60 (3) (2010) 572-590.

[20] M. Toloui, B. Firoozabadi and M. S. Saidi, A numerical study of the effects of blood rheology and vessel deformability on the hemodynamics of carotid bifurcation, *Sci. Iran.*, 19 (1) (2012) 119-126.

[21] F. Kabinejadian and D. N. Ghista, Compliant model of a coupled sequential coronary arterial bypass graft: Effects of vessel wall elasticity and non-Newtonian rheology on blood flow regime and hemodynamic parameters distribution, *Med. Eng. Phys.*, 34 (7) (2012) 860-872.

[22] M. K. Banerjee, R. Ganguly and A. Datta, Effect of pulsatile flow waveform and womersley number on the flow in stenosed arterial geometry, *ISRN Biomath.*, Article ID 853056 (2012) 1-17.

[23] Z. Mortazavinia and E. G. Rad, Study of pulsatile non-Newtonian blood flow through abdominal aorta and renal arteries incorporating fluid-structure interaction, *J. Biomed. Phys. Eng.*, 2 (3) (2012) 93-102.

[24] V. M. Pereira, O. Brina, A. Marcos Gonzales, A. P. Narata, P. Bijlenga, K. Schaller, K. O. Lovblad and R. Ouared, Evaluation of the influence of inlet boundary conditions on computational fluid dynamics for intracranial aneurysms: A virtual experiment, *J. Biomech.*, 46 (9) (2013) 1531-1539.

[25] S. M. Abdul Khader, A. Ayachit, R. Pai, K. A. Ahmed, V. R. K. Rao and S. G. Kamath, FSI simulation of increased severity in patient specific common carotid artery stenosis, *3rd International Conference on Mechanical, Electronics and Mechatronics Engineering,* Abu Dhabi (UAE) (2014).

[26] J. Xiang, A. H. Siddiqui and H. Meng, The effect of inlet waveforms on computational hemodynamics of patient-specific intracranial aneurysms, *J. Biomech.*, 47 (16) (2014) 3882-3890.

[27] G. J. Harrison, T. V. How, R. J. Poole, J. A. Brennan, J. B. Naik, S. R. Vallabhaneni and R. K. Fisher, Closure technique after carotid endarterectomy influences local hemodynamics, *J. Vasc. Surg.*, 60 (2) (2014) 418-427.

[28] M. Blagojevic, A. Nikolic, M. Zivkovic, M. Zivkovic and G. Stankovic, A novel framework for fluid/structure interaction in rapid subject-specific simulations of blood flow in coronary artery bifurcations, *Vojn. Pregl.*, 71 (3) (2014) 285-292.

[29] K. Gayathri and K. Shailendhra, Pulsatile blood flow in large arteries: comparative study of Burton's and McDonald's models, *Appl. Math. Mech. (-Engl. Ed.)*, 35 (5) (2014) 575-590.

[30] T. Meirson, E. Orion, C. Di Mario, C. Webb, N. Patel, K. M. Channon, Y. Ben Gal and D. P. Taggart, Flow patterns in externally stented saphenous vein grafts and development of intimal hyperplasia, *J. Thorac. Cardiovasc. Surg.*, 150 (4) (2015) 871-878.

[31] J. Fan, Y. Wang, J. Liu, L. Jing, C. Wang, C. Li, X. Yang and Y. Zhang, Morphological-hemodynamic characteristics of intracranial bifurcation mirror aneurysms, *World Neurosurg.*, 84 (1) (2015) 114-120.

[32] *Theory and modeling guide*, Volume III: ADINA CFD & FSI, Help of ADINA software (2011).

[33] A. Razavi, E. Shirani and M. R. Sadeghi, Numerical simulation of blood pulsatile flow in a stenosed carotid artery us-

ing different rheological models, *J. Biomech.*, 44 (11) (2011) 2021-2030.

[34] T. J. Pedley, *The Fluid Mechanics of Large Blood Vessels*, Cambridge University Press, Cambridge (1980).

[35] W. Y. Chan, Y. Ding and J. Y. Tu, Modeling of non-Newtonian blood flow through a stenosed artery incorporating fluid-structure interaction, *ANZIAM J.*, 47 (2007) 507-523.

[36] Y. I. Cho and K. R. Kensey, Effects of the non-Newtonian viscosity of blood on flows in a diseased arterial vessel, Part 1: Steady flows, *Biorheology*, 28 (3-4) (1991) 241-262.

[37] E. W. Merril, C. S. Cheng and G. A. Pelletier, Yield stress of normal human blood as a function of endogenous fibrinogen, *J. Appl Physiol.*, 26 (1) (1969) 10-23.

[38] B. M. Johnston, P. R. Johnston, S. Corney and D. Kilpatrick, Non-Newtonian blood flow in human right coronary arteries: steady state simulations, *J. Biomech.*, 37 (2004) 709-720.

[39] R. B. Bird, R. C. Armstrong and O. Hassager, *Dynamics of polymer liquids*, 2nd Ed., Wiley, New York (1987).

[40] Y. C. Fung, *Biomechanics: Mechanical Properties of Living Tissues*, 2nd Edition, Springer, Berlin (1993).

[41] P. D. Ballyk, D. A. Steinman and C. R. Ethier, Simulation of non-Newtonian blood flow in an end-to-end anastomosis, *Biorheology*, 31 (5) (1994) 565-586.

[42] W. R. Mower, W. J. Quinonse and S. S. Gambhir, Effect of intraluminal thrombus on abdominal aortic aneurysm wall stress, *J. Vasc. Surg.*, 26 (1997) 602-608.

[43] D. Zeng, E. Boutsianis, M. Ammann and K. Boomsma, A study on the compliance of a right coronary artery and its impact on wall shear stress, *J. Biomech. Eng.*, 130 (4) (2008) Article ID 041014.

[44] M. R. Sadeghi, Numerical simulation of blood flow in vessels with arterial stenosis considering fluid structure interaction*, Ph.D. Thesis*, Graduate school of Mechanical Engineering, Isfahan University of Technology (2013).

[45] S. Fazli, E. Shirani and M. R. Sadeghi, Numerical simulation of LDL mass transfer in a common carotid artery under pulsatile flow, *J. Biomech.*, 44 (1) (2011) 2021-2030.

Mehdi Jahangiri is Ph.D. student of Mechanical Engineering at Isfahan Universit of Technology, Iran. His current research interests include biomechanical and renewable energy.